Journal Article

Ultra-high-speed motor with enhanced cooling for cordless vacuum cleaners

Dianov, A., Woo, H.-M., Sun, X., Yang, R., Xiang, J., and Vagapov, Y.

Ultra-high-speed motor with enhanced cooling for cordless vacuum cleaners

Anton Dianov, *Senior Member, IEEE*, Hyeon-Myeong Woo, Xiaodong Sun, *Senior Member, IEEE*, Rui Yang, Jiawei Xiang, *Senior Member, IEEE* and Yuriy Vagapov, *Member, IEEE*

***Abstract*- Recent advancements in battery materials have significantly improved their charge-to-weight ratio providing fast progress in battery-dependent technologies and expanding the market for cordless devices in particular. Cordless vacuum cleaners have become especially popular due to enhanced convenience compared to wired models. This growing demand has boosted research activity toward further size and weight reduction. As a result, motors and impellers have been considerably scaled down to just a few centimeters in diameter, while the operating frequency of ac voltage applied to energize the motors is now increased to exceed 2 kHz. However, the reduced size and mass of the motor metal components have negatively affected cooling efficiency, making heat dissipation a major challenge in the development of compact, high-speed motors. To overcome this thermal issue, this paper proposes a novel motor design having a six-pointed star-shaped stator with toroidal windings placed at its vertices. This configuration increases the stator surface area ensuring the improvement of the heat dissipation. Moreover, the enlarged spacing between windings improves cooling conditions allowing the motor to conduct higher current through the stator windings without overheating. A working prototype of the proposed motor was developed and tested to evaluate its performance and thermal characteristics. An experiment-based comparative analysis with commercial vacuum cleaner motors showed that the prototype outperformed them in both operational and thermal parameters confirming the effectiveness of the proposed concept.**

***Index Terms*—High speed motors, Permanent magnet motors, Brushless machines, Stators, Energy efficiency**

I. Introduction

Over the past few decades, electric transportation systems have been extensively developed as a response to the growing demand for CO_2 emission reduction [1]. Following this trend, technologies related to electric vehicles (EVs) have made significant progress, particularly in battery advancements [2]. Major improvements in battery cost, size, and capacity have facilitated battery implementation in other areas, boosting the production of various autonomous and cordless devices for both industrial and domestic applications [3]. A notable example is the increasing popularity of cordless vacuum cleaners (VCs), which have gained attention for their enhanced mobility and convenience [4].

Although cordless vacuum cleaners are more expensive than conventional wired VCs, they are becoming increasingly attractive to customers. Bi and Shao [5] reported that, as of today, the customer selection rate for cordless VCs has reached 85% in Europe and America, while Lin et al. [6] predict a massive increase in market value, rising to $20 billion by 2030. Due to the growing demand for cordless VCs, significant efforts have been made to develop, improve, and optimize these devices by reducing size and weight, increasing rated power, and enhancing operational efficiency [7]-[9].

The electric motor drive generating suction power at the airflow intake is the most critical component of a vacuum cleaner (VC) as it directly determines the device performance. Universal motors commonly used in wired VCs [10], are increasingly being replaced in modern cordless models by permanent magnet synchronous motors (PMSMs) operating often as brushless DC (BLDC) motors [11]. Application of PMSMs enables high-speed operation to meet the demanding requirements for compact size, low weight, and high power efficiency in cordless designs. Typical motor speeds in modern cordless VCs exceed 100,000 rpm [12]. Running at such high speeds, the motor can be made a small and lightweight component while still delivering high suction power, despite developing relatively low torque at the shaft [13]. High suction power is essential for ensuring effective cleaning performance, as it provides sufficient force to remove microscopic particles from a wide range of cleaning surfaces.

A specific feature of VC motor drives is the forced air-cooling mechanism where the airflow generated by the impeller is arranged to move through the motor. Due to high-speed airflow, this approach provides direct and efficient cooling of the motor without any heatsink installation [14]-[16].

Significant effort is applied to the optimization of motor design for cordless VCs focusing on both size/weight reduction and power increase. This leads to a substantial rise in power density, as the motor diameter is reduced to just a few centimeters while the rated power increases to 500–600 W. A typical PMSM rotating the impeller of a cordless VC operates at frequencies exceeding 2 kHz, with phase currents reaching 40–50 A. Iron power losses occurred in the motor operating at a high-speed and high currents through the stator windings significantly contribute to motor heating whereas the small motor size worsens heat dissipation. Despite the high-speed airflow through the motor drive, improving

Anton Dianov and Rui Yang are with the Pingyang Institute of Intelligent Manufacturing, Wenzhou University, Wenzhou, 325400, China (e-mail: anton@wzu.edu.cn, 20210272@wzu.edu.cn).

Hyeon-Myeong Woo is with Department of Electrical and Electronics Engineering of Pusan National University, Pusan, South Korea (e-mail: glsald@pusan.ac.kr)

Xiaodong Sun is with the Jiangsu University, Automotive Engineering Research Institute, Zhenjiang, China (e-mail: xdsun@ujs.edu.cn).

Jiawei Xiang is with Wenzhou University, College of Mechanical and Electrical Engineering, Wenzhou, China (jwxiang@wzu.edu.cn).

Yuriy Vagapov is with the Faculty of Arts, Computing and Engineering, Wrexham University, Wrexham, LL11 2AW, UK, (e-mail: yuriy.vagapov@wrexham.ac.uk).

cooling conditions and heat transfer remains a crucial issue for continued progress in VC development [17]-[21].

The market leaders in the development and implementation of PMSMs for VCs are Dyson, Samsung, and LG. These companies are actively engaged in the research and development of state-of-the-art motor drive technologies to achieve enhanced performance characteristics such as higher rotational speeds, increased suction power, effective thermal management, and reduced acoustic noise. The motor drives offered by these manufacturers are varied in design structure but all ensure high-speed operation. Fig. 1a illustrates comparable motors with impellers produced by the major VC manufacturers and Fig. 1b shows cross-section areas of the motor stators. LG and Samsung [22] employ three-phase configurations in their high-speed motors with slot/pole combinations of 3/2 and 6/4, respectively. In contrast, Dyson uses a single-phase motor with four stator slots and an eight-shoe, eight-pole design [26]. This configuration ensures the increase in the heat exchange surface area for cooling airflow, offering improved thermal management in comparison to conventional three-phase motors. The main design parameters of the motors are shown in Table I. The tabulated data demonstrate that the stack length of the Samsung and LG motors is much shorter compared to their outer diameter (excluding Dyson) indicating that this form factor was likely selected as a solution to overcome thermal issues.

The comparison of the analyzed motors demonstrates that the motor design (particularly the configuration of the motor body surface) has a significant impact on cooling performance and, therefore, on the operational temperature of the motor body. As mentioned above, one of the most critical factors influencing thermal behavior is the effective cooling surface area of the stator. Table I presents this parameter for the

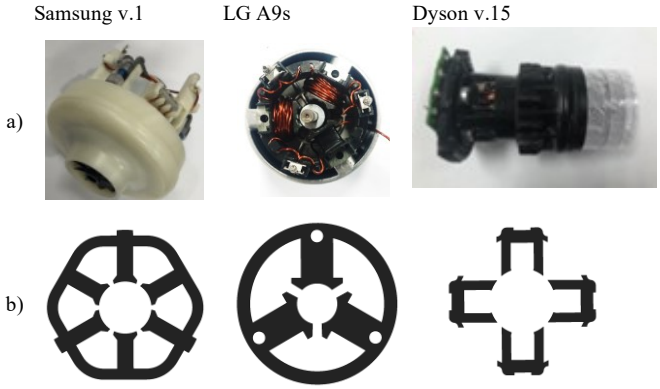

Fig. 1. Competitive motors. a) Motor with impeller; b) Stator cross-section

TABLE I. COMPETITIVE VC MOTORS

Parameters	Samsung v.1	LG A9s	Dyson v.15
Slot/poles	6/4	3/2	4/8
Stack length, mm	9	9.5	18
Outer/inner diameters, mm	42/15	47/11	24/10
Cooling contour, mm	185	295	178
Cooling surface, mm^2	1663	2805	2477
Number of phases	3	3	1
Weight, g	205	232	175
Rated voltage, V	21.6	25.2	25.2

competing motors, analytically derived from their physical dimensions. Only the metallic surfaces in direct contact with the cooling airflow are considered. These values do not consider variations in surface cooling efficiency due to metal surface properties or airflow distribution. It should be noted that more complex motor designs providing enhanced heat dissipation often result in substantially higher manufacturing costs [29], [30].

This study proposes a new motor design which can significantly improve motor thermal performance and offer a cost-efficient solution. The main contribution of this study includes:

♦ Development of an innovative stator design specifically for VC motors. This new design provides better heat dissipation compared to existing high-speed motor configurations,

♦ Experimental validation of the stator thermal performance under various operating conditions corresponding to real-world usage,

♦ Definition of the maximum level of power at which the motor can operate without exceeding acceptable temperature limits to ensure reliable motor performance and extended lifetime,

♦ Comparative experimental analysis conducted on several comparable motors to benchmark the proposed motor design where thermal characteristics were used as the primary evaluation criterion.

II. THERMAL ISSUES IN HIGH-SPEED MOTORS

A. Stator Thermal Consideration

The thermal condition of a PMSM significantly depends on the power losses occurring in the stator when the motor operates under load conditions. This power is converted into heat and must be transferred from the motor body surface to the ambient (air). As in any conventional electrical machine, the power losses generated in the PMSM stator consist of iron losses in the laminated stator stack (P_{Fe}) and copper losses in the stator windings (P_{Cu}). In high-speed motors, the increased frequency of AC voltage applied to the stator windings is a major factor contributing to higher iron losses. Copper losses are related to the motor load and depend on the current density in the stator windings. Typical current density values range from 1 to 10 A/mm² for conventional motors. However, in high-speed applications, the limit in the current density can be massively increased up to 30-40 A/mm^2 due to higher insulation class and intensive forced-air cooling arrangements [31].

Due to compact design, high-speed motors are designed to operate at high power density, which can potentially lead to overheating. Therefore, the combination of both power losses in the stator must not exceed the heat dissipation limit (the amount of power the motor can effectively transfer to air) to keep the motor temperature below the permissible value.

$$P_{Fe} + P_{Cu} \le P_s, \tag{1}$$

where P_{Fe} is the power loss in the laminated stator stack; P_{Cu} is the power loss in the stator windings; P_s is the maximum value of the heat dissipated from the external surface of the stator.

The iron loss in the laminated stator stack for a given type of steel is typically expressed as a power function of the magnetic field density B_m and the frequency f. The commonly used expression for iron loss is as follows:

$$P_{Fe} = k_h f B_m^{\alpha} + k_e \left(f B_m\right)^2 + k_a \left(f B_m\right)^{1.5}, \quad (2)$$

where k_h is the hysteresis loss coefficient; k_e is the eddy loss coefficient; k_a is the abnormal loss coefficient.

The copper losses are proportional to I^2R, where I is the current in the winding and R is the winding resistance. Copper loss depends significantly on the value of the current, while the resistance varies with the wire temperature increasing as the temperature rises.

The maximum heat dissipation corresponding to a certain permissible temperature is defined as follows:

$$P_s = h\left(\vartheta_m - \vartheta_a\right)\pi D_e l_s, \quad (3)$$

where h is the heat transfer coefficient (the value is variable and depends on the cooling process conditions); ϑ_m is the maximum permissible motor temperature; ϑ_a is the ambient (air) temperature; D_e is the external diameter of the stator; l_s is the length of the stator.

B. Heat Transfer and Suction Process Challenges

In high-speed motor design, the heat transfer coefficient h is often assumed to be around 100 W/(°C·m²) [32], [33]. This value is typically related to forced air-cooling systems, where the speed of air employed as a heat transfer agent is directly linked to the motor rotational speed. However, this coefficient is a complex parameter depending on a combination of various factors, including airflow velocity and air density. These factors can vary significantly in VC applications where the conditions of the suction process are variable and unstable.

Both domestic and industrial VCs usually operate under inconstant inlet conditions; it depends on factors such as the type of nozzle used, the proximity of the inlet to the surface being cleaned, clogged air filters, full dust container, and potential blockages caused by debris or obstacles. A reduction in the inlet area leads to decreased airflow through the motor for cooling, as less air is drawn into the cleaner. Simultaneously, the internal air pressure drops reducing the density of air circulating in VC. For example, full blockage of the air inlet reduces the air pressure inside VC chamber in a range of 15 to 25 kPa below atmospheric pressure [6].

Both of these factors (reduced airflow speed and lower air density) negatively affect the motor cooling efficiency. Specifically, this negative influence is expressed in the form of reducing the heat transfer coefficient making the removal of the heat from the stator surface more difficult. According to equation (3), this decline in the stator heat dissipation capability can lead to rapid motor overheating.

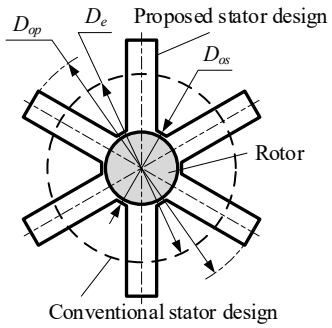

Fig. 2. Schematic comparison of stator surface area for conventional (cylindric) design and proposed solution

Despite the low power drawn by the motor when low air pressure occurs in VC chamber due to a reduced or blocked inlet, the motor can overheat because the cooling conditions of low air density are significantly decreased. Under these circumstances, if the motor is not properly designed, the protection system often shuts it down to prevent overheating, fire, or other catastrophic failures in compliance with health and safety regulations. This makes the practical use of such VCs inconvenient negatively impacting customer experience and affecting market sales.

C. Concept of Stator Surface Enlargement

Equation (3) is applicable for a conventional high-speed motor design, where the stator is approximated as a cylinder and the surface area involved in heat transfer is calculated as $S = \pi D_e l_s$. It can be seen that the surface area is the most influential parameter affecting the motor thermal condition. Hence, under the same heat dissipation limit and heat transfer coefficient, increasing the surface area ensures reducing the motor temperature.

Any approach used to extend the surface area of the motor stator inevitably requires modifications to the stator design, including changes to the laminated stator stack layout and the winding installation configuration. The concept proposed in this paper for increasing the stator surface area involves converting the cylindrical form of the stator into a star-shaped configuration, where the windings are installed in a toroidal arrangement at the end of each point of the star. Various types of stars can be applied as a basis for stator modification to enlarge the surface for the cooling condition improvement.

Fig. 2 illustrates a proposal on how the heat transfer surface area of the stator can be increased in high-speed motors. It demonstrates that the rearrangement of the stator windings and the modification of the laminated stator stack into a six-pointed star-shaped configuration significantly enlarge the surface area compared to a conventional “cylindrical” motor design. Considering two motors with the same rated power but different stator configurations (“cylindrical” and “star”), an increase in the surface area involved in the heat transfer improves the motor thermal performance. Despite some minor drawbacks, this approach is considered a promising solution for high-speed motor design, as it effectively contributes to temperature reduction.

The increase in surface area for the proposed stator design can be estimated using the following approach. It is assumed that the conventional "cylindrical" motor and the proposed design have similar power output and the same stator length l_s. The surface area of the proposed motor can then be approximately defined as follows:

$$S_p = \pi D_{os} l_s + 6\left(D_{op} - D_{os}\right) l_s, \quad (4)$$

where S_p is the stator surface area of the proposed design available for heat transfer, D_{os} and D_{op} are the shoe and pole outer diameters of the six-pointed star-shaped configuration.

Therefore, the ratio S_p/S indicating the increase in stator surface area of the proposed design relative to the conventional motor is determined as follows.

$$\frac{S_p}{S} = \frac{D_{os}}{D_e} + 6\frac{\left(D_{op} - D_{os}\right)}{\pi D_e} \quad (5)$$

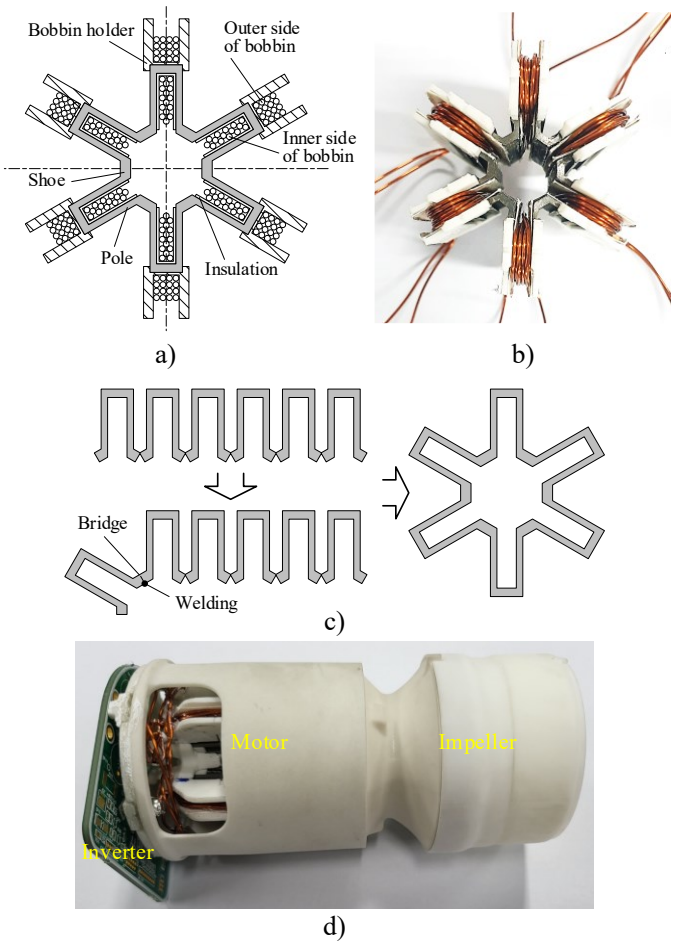

Fig. 3. Designed motor. a) Stator cross-section; b) Assembled stator; c) Stator stack assembling; d) Assembled vacuum cleaner drive

TABLE II. PARAMETERS OF THE PROPOSED PROTOTYPE

Parameters	Proposed motor
Slot/poles	6/2
Stack length, mm	28
Outer/inner diameters, mm	30/10
Cooling contour, mm	251
Cooling surface, mm^2	7022
Number of phases	3
Weight, g	182
Rated voltage, V	25.2

According to equation (5), the surface area available for cooling in the proposed motor design is approximately 2-2.5 times higher than that of the conventional motor.

However, it should be noted that this analytical approach provides approximate figures, as the actual surface area of the star-shaped stator is not ideal as assumed for the equation (5). The stator design includes various plastic and metal components, fixing elements, and winding holders which affect the overall surface area available for forced air cooling.

III. PROPOSED MOTOR DESIGN

A. Stator Configuration

A novel motor designed using the approach discussed above is proposed and illustrated in Fig. 3. Fig. 3a shows a cross-sectional view of the stator which is modified to increase the surface area used for cooling by forced airflow. It can be seen that the stator configuration follows the six-pointed star-shaped concept for surface enlargement. Table II presents the cooling surface value for comparative analysis with the corresponding data from other motors (Table I).

The motor has six slots, while the rotor is two-pole. The slots in the proposed motor configuration are designed to be flat and long, which significantly enhances the overall cooling surface area. Additionally, the inner thickness of the slots is very thin. This specific feature allows for the flat arrangement of the winding wires inside the slot. Fig. 3a also shows that the inner side of the bobbin is thinner than the outer side, which improves heat transfer from the windings located inside the slot to the laminated core stack.

Fabricating star-shaped laminations for stack assembly is obviously not economically viable due to poor utilization of the electrical steel sheet. To improve production efficiency and minimize material waste, the following approach is applied for stator stack manufacturing. First, the stator lamination is cut as a strip to maximize the use of the electrical steel sheet. Then, the stack of laminations is bent and welded, as shown in Fig. 3c, to form a star-shaped stator. This method of fabricating a star-shaped stator stack is both efficient and cost-effective.

A conventional approach to increasing the power of electric motors is to extend the laminated core stack to make the motor body longer. The proposed stator design supports longer lengths of stator stacks enabling higher motor power compared to conventional designs with shorter motor bodies. An additional advantage of the implementation of a longer lamination stack is the reduction in the percentage of the frontal winding sections which improves copper utilization.

The stator in the proposed design is made of non-oriented magnetic steel Super Core 10JNHF600 with a lamination thickness of 0.1 mm.

B. Stator Windings

The key feature of this new design is the use of toroidal stator windings, which are spaced apart from one another. Toroidal windings are often used in high-speed motors with conventional stator designs [31], [34]. In the proposed stator

configuration, the toroidal windings are embedded in the stator slots in such a way that the windings remain significantly separated. This separation effectively prevents mutual thermal influence between the winding coils and provides an increased cooling surface around each source of heat.

As shown in Fig. 3a, the winding arrangement is asymmetrical: the outer side of the bobbin is designed to cover all outer surfaces of the slot, while the inner side of the bobbin lies flat within the thin slot. This asymmetry serves two purposes: it helps suppress stray magnetic fields and increases the surface area exposed to airflow which enhances cooling efficiency. The improved thermal performance resulting from this asymmetrical winding design allows for a higher current density, which increases the power-to-weight ratio of the proposed motor.

The stator assembly is shown in Fig. 3b; it illustrates the major components of the stator: laminated core stack and three-phase windings embedded into the slots of the stator. Each phase of three-phase winding consists of two parallel coils with 14 turns of copper wire with a cross-sectional area of 1.1 mm^2.

C. Motor Drive

The proposed motor was designed and built as a working prototype. Fig. 3d shows the complete motor drive equipped with an inverter mounted on the left side of the motor. The right side of the motor is connected to the impeller, which provides airflow for VC and, consequently, for motor cooling. The impeller inlet is connected to the motor creating a suction airflow passing through the motor. The parameters of the motor drive prototype are summarized in Table II.

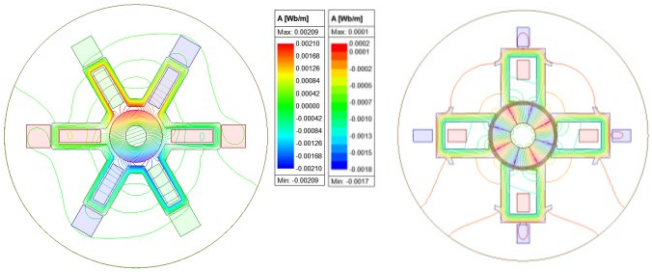

a) b)

Fig. 4. Distribution of the magnetic vector potential: a) Proposed motor; b) Dyson v.15

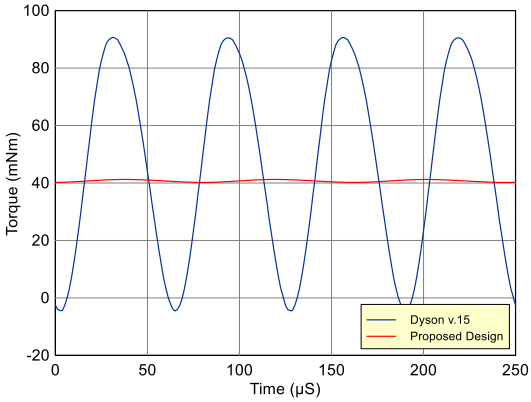

Fig. 5. Torque ripple comparison: Proposed motor drive vs. Dyson motor.

TABLE III. RESULTS OF FEM MODELLING

Parameters	Proposed motor	Dyson v.15
Speed, rpm	122,000	120,000
Torque (average), mNm	40.7	46.5
Torque (peak-to-peak), mNm	1.0	95.3
Torque (ripple), %	2.45	205
Eddy Current Loss, W	1.75	8
Core Loss, W	6.0	12.6

This design, in which the inverter is mounted directly on the motor and the motor terminals are soldered to the PCB, is widely adopted by many manufacturers due to its several advantages, such as the following. No connection wires and connectors are required between the motor and the inverter circuit, as the motor winding wires are directly soldered to the inverter PCB. The exclusion of wires and connectors reduces overall cost, enhances compactness and simplifies assembling. Additionally, the short electrical connections reduce voltage stress caused by fast commutations and high dv/dt. This also helps to prevent overvoltage at motor terminals, which may occur due to the reflected wave phenomenon in drives with long connection cables [23, 24]. Mounting the inverter PCB directly on the motor body also ensures effective cooling of the inverter electronic switches, as the PCB is located in the airflow generated by the motor impeller. Due to this efficient cooling, a heat sink is not required, resulting in savings in cost, space and weight [25].

The motor drive is designed to operate at speeds exceeding 120 krpm, with testing conducted at 135 krpm. Since the motor uses a two-pole rotor, the frequency of ac voltage required to power the motor exceeds 2 kHz. Such high frequency increases iron losses compared to conventional low-frequency motors. Additionally, the design slightly extends the magnetic path in the stator, which can further contribute to increased iron losses and may negatively impact overall motor efficiency. Moreover, the proposed flat-slot stator configuration requires a larger volume of active materials potentially reducing the power-to-weight ratio. To assess the trade-offs between the advantages and drawbacks of the proposed design, a working prototype of the motor drive was tested alongside other competitive motors. The testing procedure and results are presented in Section IV.

The proposed motor design is loosely similar to the high-speed motor produced by Dyson for VC applications [26]. However, the Dyson motor is a single-phase drive, whereas the proposed device is a three-phase motor. Although the stator of the Dyson motor has toroidal windings to enhance thermal management, its laminated core stack is split into four independent sections (Fig. 1b) to enable a single-phase power supply configuration. These mechanically separated parts are held together using a plastic compound, forming the stator into a single unit. However, the plastic compound used to bond these four parts covers areas of the stator surface where heat is generated. This reduces the efficiency of heat dissipation and negatively impacts the motor's thermal performance. In contrast to the Dyson solution, the proposed motor has a laminated stator manufactured as a single mechanical unit (Fig. 3c), which requires no plastic components for core

assembly and therefore provides better conditions for heat transfer.

D. Numerical Modelling

The proposed motor drive was numerically modelled and simulated using Ansys to determine the torque ripples and core power losses. Since the proposed motor is loosely similar to the Dyson motor, the modelling and simulation were also focused on the comparison analysis of these two motors. Fig. 4 shows the results of the FEM simulations for both motors, demonstrating the distribution of the magnetic vector potential in the magnetic circuits. The created numerical models were used to investigate the operational performance of each motor in terms of both torque ripples and power loss. The results obtained from numerical modelling and simulation are summarized in Table III.

The advantage of three-phase motors is their significantly lower torque ripples compared to single-phase motors. In fact, single-phase motors operate in a pulsing torque mode, leading to higher electromagnetic fluctuations. The torque waveforms for both the Dyson motor and the proposed drive are shown in Fig. 5. It can be observed that, despite having comparable average torque values, the peak-to-peak variations are significantly different (1.0mNm for the proposed drive versus 95.3mNm for the Dyson motor). Therefore, simulation results indicate that the proposed three-phase motor has a torque ripple of only 2.45%, whereas the single-phase Dyson motor reaches 205%. The pulsing current associated with such high torque ripple substantially increases losses in the motor magnetic materials. According to the data obtained from the numerical analysis, the proposed motor demonstrates eddy current losses lower by 3-4 times compared to the Dyson motor.

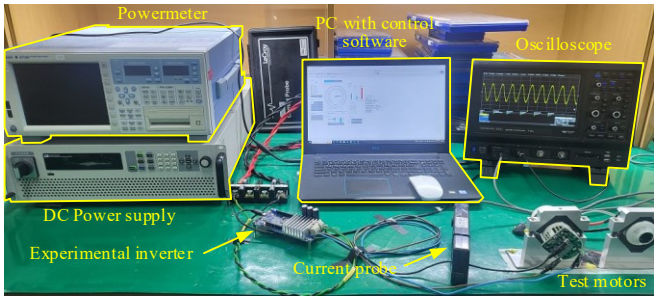

Fig. 6. Test rig for motor signals evaluation.

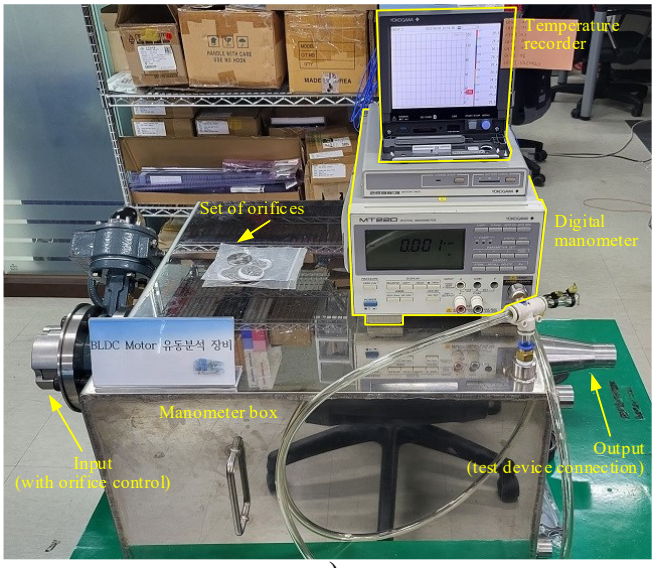

a)

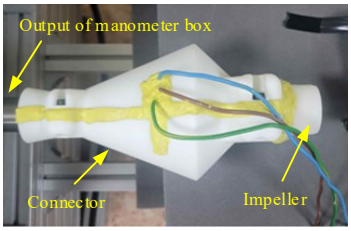

b)

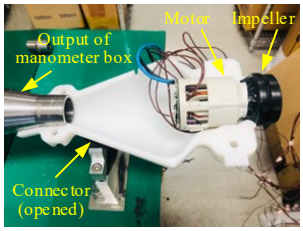

c)

Fig. 7. Test rig for VC motor drive performance evaluation. a) Equipment; b) Motor with impeller, connected to the manometer box; c) Opened connector

IV. Experimental Investigation

A. Testing Equipment

To operate the designed motor prototype, the evaluation inverter board EVSPIN32G4 based on the STSPIN32G4 microcontroller was used. The board was connected to a PC via a USB interface which was used for control communication and data monitoring. The motor control software implemented sensorless field-oriented control (FOC) and was developed using rapid prototyping software provided by STMicroelectronics. The FOC software was further enhanced with additional control algorithms to increase system efficiency and perform smooth starting. The structure of the resulting control scheme is described in detail in [27], while the open-loop starting and instant closing operations are discussed in [28].

The competitive motor drives were evaluated using their native control algorithms. The control strategies of these commercial motors are protected under intellectual property rights and can only be assumed through analysis of their experimental behavior. The LG motor appears to use a conventional FOC scheme with a speed control loop. For the Samsung motor, where the speed is varied while the power remains relatively stable, it is likely that an FOC strategy with a “constant-power” loop is implemented. The Dyson motor seems to employ rectangular control with current limitation, which is a typical approach for single-phase motor drives.

The experimental motor drive was powered by Techway Kewell power source C3000H, which is connected to a PC via USB to provide power control functions. All electric power measurements were conducted using a Yokogawa WT1800 power analyzer, while voltage and current waveform signals were recorded using a Yokogawa DL-850 digital oscilloscope, capable of capturing both images and raw data. The testing equipment set-up used for motor operation and electrical parameters evaluation is shown in Fig. 6.

A specific test rig was arranged to conduct practical experiments to investigate the parameters of the proposed motor prototype and competitive motors from other

manufacturers for comparative analysis. To assess the performance and heating behavior of various VC motor drives, the test rig shown in Fig. 7a was used. It includes a manometer box and a tube for pressure measurement connected to a digital manometer. The inlet of the manometer box is controlled by interchangeable orifices of different diameters to simulate VC load. The VC motor drives under test were connected to the output of the manometer box using a custom-designed connector as shown in Fig. 7b. To avoid air leakage and reduce measurement errors, all gaps in the connector are coated with yellow sealant. Fig. 7c shows the same connector in the opened state, illustrating the internal wiring and motor installation. This setup corresponds to the temperature rising test, in which additional wires with thermocouples are connected to the motor. The temperature of the motor windings was measured using thermocouples attached to the outer surface of the bobbins and recorded using a Yokogawa FX1000 data recorder.

It should be noted that Fig. 7b and Fig. 7c show black and white impellers installed on the motor shaft. While both impellers have a similar design, their aerodynamic characteristics are slightly different. During testing, the impellers were evaluated to identify the most suitable prototype for the developed motor.

B. Experimental Procedures

To verify the feasibility of the proposed design, a series of experiments was conducted to compare it with existing motor drives available on the market as components for VCs. In all tests, the competitive motor drives were powered using their original inverters and operated under the control algorithms provided by their manufacturers. This ensured that the motors were tested under optimal conditions as intended by the motor developers. The proposed prototype was tested using a specially developed inverter and operated under an appropriate control algorithm tuned specifically for efficiency optimization.

Initially, the motor drive prototype was tested to investigate its performance characteristics under various speed and load conditions. The data obtained from these tests are presented as motor performance curves in Fig. 8, showing the phase current (rms) and input power versus motor rotational speed. The waveforms of the phase current under both no-load and full-load conditions at a rotational speed of 120 krpm are shown in Fig. 9. The waveform of the back EMF measured at the rotational speed of 37,74 krpm is demonstrated in Fig. 10. These waveforms are visual representations of the readings measured and recorded by the test rig instruments during the execution of the tests.

In the first series of experiments conducted for comparative analysis purposes, both the commercial motors and the proposed prototype were tested to evaluate their electrical characteristics and suction power at the rated rotational speeds. The suction power in Air Watts (AW) was calculated using vacuum pressure and airflow readings obtained from the test rig instrumentation. The measurements

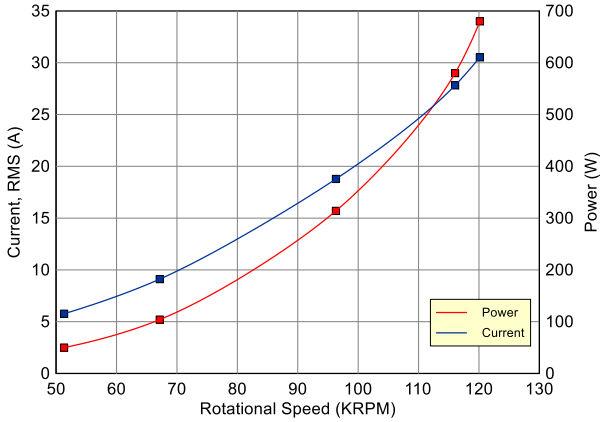

Fig. 8. The motor performance characteristics: phase current (rms) and input power vs. rotational speed.

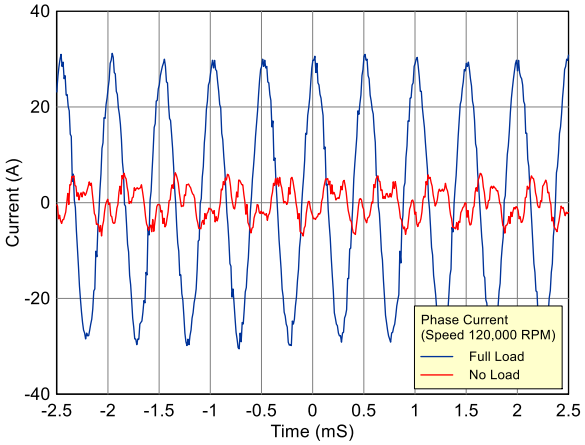

Fig. 9. Waveforms of the phase current for no-load and full-load conditions at the rotational speed of 120 krpm.

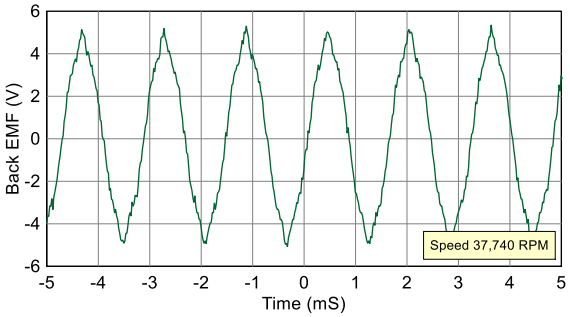

Fig. 10. Waveform of the back EMF at the rotational speed of 37.74 krpm.

TABLE IV. COMPARISON OF VARIOUS VC MOTORS

Parameters	Samsung v.1	LG A9s	Dyson v.15	Proposed
Suction power, AW	200	210	240	280
Input power, W	550	590	660	740
Maximum speed, krpm	75	115	125	135
Current density, A/mm^2	15.9	20.7	36.3	32.0
System efficiency, %	36.6	35.6	36.4	37.8
Power/Weight, AW/g	0.976	0.905	1.314	1.538
Suction power, AW	200	210	240	280
Input power, W	550	590	660	740

obtained from the test equipment are shown in Table IV. This table presents the key parameters of each motor investigated in this series of experiments; the provided data are the basis for a motor comparative analysis.

The second series of experiments focused on evaluating the thermal performance of the motors. Each motor under the

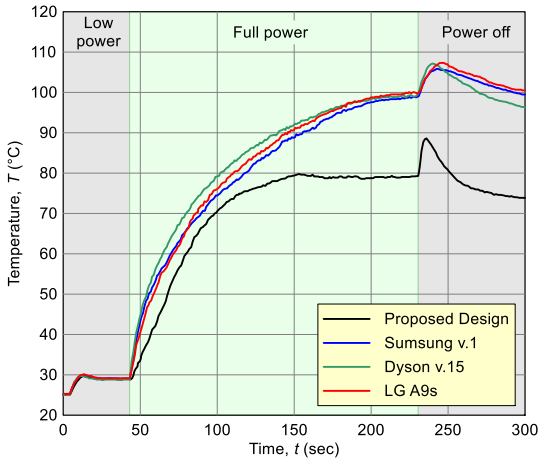

Fig. 11. Temperature transient tests for competitive and proposed motors

test was equipped with a thermocouple installed on the outer surfaces of the stator windings to measure the winding temperatures and observe temperature transients under varying operating conditions. However, it was recognized that due to effective cooling by airflow during normal motor operation, this method is inaccurate providing lower temperature readings than those inside the windings. To estimate the internal winding temperature, the test procedure included switching off the motor power after full-power operation when the thermal steady state condition in the stator windings was reached. Since the impeller stops when the motor is de-energized, forced airflow through the motor is also stopped allowing the outer winding temperature to rise rapidly to achieve the inner temperature. This temperature rise is held for a short period of time and can be observed as a pick on the temperature vs. time curve. This peak value is clearly visible on the temperature transient graph and reflects the actual internal winding temperature during full-power operation.

Fig. 11 demonstrates a family of the temperature curves recorded for all tested motors including the proposed prototype. All motors initially operated under low power for 45 sec. followed by full-power operation for approximately 180 sec. to reach thermal steady state condition. After this, the motors were switched off to observe the temperature peak representing the internal winding temperature. The room temperature during all tests was maintained at a constant 25°C.

V. Discussion

The performance characteristics of the motor prototype shown in Fig. 8 demonstrate typical behavior of a motor drive operating with a centrifugal load. It can be observed that the shapes of both curves, phase current (rms) and input power versus rotational speed, follow a power function, which is commonly associated with air impeller performance. This confirms that the motor prototype is well-suited to drive an impeller in VC applications and is fully capable of generating sufficient airflow to provide an efficient suction process.

Fig. 9 shows the waveforms of the phase current of the motor drive prototype operating under no-load and full-load conditions at the same speed of 120 krpm. The currents were recorded by the instrument and visualized to demonstrate the shape and confirm the current frequency of 2 kHz. It can be observed that the periodic time of both waveforms is $T = 0.5\ ms$ which, for a two-pole motor, corresponds to the rotational speed of the prototype of 120 krpm. ($n = 60/T = 60/0.5\times10^{-3} = 120{,}000$ rpm). Fig. 9 also demonstrates that, in contrast to the sinusoidal current under full-load conditions, the shape of the current waveform under no-load conditions significantly differs from a sinusoidal form. This can be explained by reduced measurement accuracy at low current values and the low inertia of the motor under no-load conditions, which makes the current highly sensitive to torque variations.

The frequency of the back EMF waveform shown in Fig. 10 is 629 Hz, which corresponds to a rotational speed of 37.74 krpm. The graph demonstrates a sinusoidal shape of the back EMF and a low level of higher harmonics, confirming the correct design of the motor drive prototype.

The results presented in Table IV demonstrate the characteristics obtained from experiments conducted on four motors: three commercially available models and the proposed prototype. Despite having the highest input power (740 W), the proposed motor shows excellent performance in several important areas including suction power (280 AW), maximum rotational speed (135 krpm), overall system efficiency (37%), and power-to-weight ratio (1.538 AW/g) outperforming all other tested motors. It also demonstrates a comparably high current density in the stator windings (32 A/mm²) being second only to the Dyson motor. Although it is expected that due to the specific stator design, the efficiency of the proposed motor may be slightly lower than the efficiency of conventional high-speed motors, the overall system, where the prototype operates at a driving component, demonstrated the best efficiency performance in the comparative tests.

The temperature transient curves for all tested motors are shown in Fig. 11. These curves indicate that the proposed motor performs similarly to the others under low-power operation. However, at the end of the full-power phase, when the steady-state condition is achieved, the winding temperature of the proposed motor is significantly lower than that of the other motors (80°C vs. 100°C). When the motors are powered off to determine the internal temperature of the windings, the proposed design again shows a considerably lower temperature compared to the others (89°C vs. 108°C).

Despite the lower winding temperature at steady-state conditions (89°C) compared to the other tested motors, insulation Class F (rated up to 155 °C) was selected for the proposed design. This choice is dictated by the UL60730 standard to comply with Class B functional safety requirements for household appliances [35], including electric motors. These requirements are essential to ensure the safe and reliable operation of the motor and to prevent potentially hazardous situations that may endanger the appliance users.

The thermal motor time constant, derived from the temperature transient curves (Fig. 11), shows that the proposed motor has a lower thermal constant (33 s) compared

to the other motors (47 s for Dyson, 56 s for Samsung, and 58 s for LG). Since the thermal constant mainly depends on the motor weight and size, this result confirms that the proposed design offers a better power-to-weight ratio than the competing motors.

The discussed findings indicate that the proposed motor performs better than other tested motors in both electrical and thermal performance. Therefore, it can be considered a possible candidate for future research and potential integration into commercial VC designs.

Future work on the proposed motor will focus on the detailed optimization of the stator design to improve cooling efficiency. This will involve optimizing the geometry of the laminated stator stack, the winding placement configuration, and exploring the use of advanced materials. The laminated stator manufacturing issues will also be the focus of future work to optimize raw laminated steel consumption.

VI. Conclusions

This paper proposes a novel motor design featuring a six-pointed star-shaped stator with toroidal windings. In this design, the increased stator surface area enhances heat dissipation, while the larger spacing between windings improves airflow and cooling.

A motor drive prototype based on the proposed design was developed and built to validate the concept of improved cooling. The prototype was tested under various load conditions and at different speeds to evaluate its performance characteristics. Particular attention was given to testing the prototype performance at a speed of 120 krpm which required AC voltage frequency of 2 kHz.

A comparative analysis was conducted using data obtained from a series of tests in which the prototype was evaluated alongside three commercially available motors offered by VC manufacturers. Thermal tests were also performed to provide comparative thermal analysis, specifically to evaluate and compare the internal winding temperatures of the industry-offered motors and the prototype.

Overall, the series of tests conducted for the comparative analysis demonstrated that the proposed motor offers better electrical and thermal performance characteristics compared to other commercially available motors from leading VC manufacturers. This makes the proposed motor design a promising candidate for further research and implementation in industry-produced VCs.

Acknowledgment

The developed VC motor drive was highly recognized by the Korean government and was awarded the 2023 New Excellent Technology Award by the Ministry of Trade, Industry and Resources of Republic of Korea.

References

[1] V. Prakht, et al., “Analysis of Performance Improvement of Passenger Car Synchronous Homopolar Generator with the Addition of Ferrite Magnets”, Appl. Sci., 13, 3990, pp. 1–19, Mar. 2023.

[2] A. Arbuzina, M. Arkharova, A. Politsinsky, G. Demidova, A. Garg and N. Poliakov, “Research and Simulation of Step-Up Converter of Battery Power Supply for DC Drive System,” Int. Symp. Power Electron., 2023, pp. 01-06.

[3] A. Spampinato, G. Forte, G. Scelba and G. De Donato, “A Cost-Effective Switched Reluctance Motor Drive for Vacuum Cleaners,” Int. Symp. Power Electron., Elect. Drives, Automat. Motion, 2020, pp. 36-41, doi: 10.1109/SPEEDAM48782.2020.9161853.

[4] Y. Xiao, et al., “Survey data on customer two-stage decision-making process in household vacuum cleaner market,” Data in Brief, vol. 54, Jun. 2024, Art. no. 110353, doi: 10.1016/j.dib.2024.110353.

[5] Q. Bi and D. Shao, “Loss analysis of high-speed permanent magnet motor for cordless vacuum cleaner,” Journal of Physics: Conference Series, vol. 2488, 2023, Art. no. 012021, doi: 10.1088/1742-6596/2488/1/012021.

[6] J. Lin, et al., “Performance testing of cordless handheld vacuum cleaners,” Aerosol and Air Quality Research, vol. 24, no. 10, Oct. 2024, Art. no. 240082, doi: 10.4209/aaqr.240082.

[7] K. B. Jang, Sung Hong Won, Tae Heoung Kim and Ju Lee, “Starting and high-speed driving of single-phase flux-reversal motor for vacuum cleaner,” IEEE Trans. Magn., vol. 41, no. 10, pp. 3967-3969, Oct. 2005, doi: 10.1109/TMAG.2005.855181.

[8] V. Prakht, V. Dmitrievskii, V. Klimarev and D. Askerov, “High speed flux reversal motor for power tool,” 6th Int. Electric Drives Production Conf., 2016, pp. 306-311, doi: 10.1109/EDPC.2016.7851347.

[9] H. Arita, K. Nishiwaki, M. Iezawa and T. Kosaka, “High speed homopolar type permanent magnet motor designed for fast acceleration response,” 23rd Int. Conf. Elect. Mach. Syst., 2020, pp. 1930-1935, doi: 10.23919/ICEMS50442.2020.9291081.

[10] V. Dmitrievskii, V. Prakht, V. Kazakbaev and S. Sarapulov, “Optimal design of a high-speed single-phase flux reversal motor for vacuum cleaners,” Energies, 11, 3334, pp. 1–13, Nov., 2018.

[11] A. Dianov, et al., “Substitution of the universal motor drives with electrolytic capacitorless PMSM drives in home appliances,” Int. Conf. Power Electron. ECCE Asia, 2015, pp. 1631–1637.

[12] K. Hu, G. Zhang, and W. Zhang, “Analysis and optimization of temperature field of high-speed permanent magnet motor,” Advances in Mechanical Engineering, vol. 14, no. 5, pp. 1–11, May 2022, doi: 10.1177/16878132221095914.

[13] A. Dianov, N.S. Kim and Y.K. Kim, “Future drives of home appliances: Elimination of the electrolytic DC-link capacitor in electrical drives for home appliances,” IEEE Ind. Electron. Mag., vol. 9, no 3, pp. 10–18, Sep. 2015. DOI: 10.1109/MIE.2014.2367051.

[14] Z Li, et al., “Loss analysis of high-speed permanent magnet motor based on energy saving and emission reduction,” Energy Reports, vol. 9, pp. 2379–2394, 2023, doi: 10.1016/j.egyr.2023.01.053.

[15] Z. Lia, P. Wang, L. Liu, Q. Xu, S. Che, L. Zhang, S. Du, H. Zhang, and H. Sun, “Loss calculation and thermal analysis of ultra-high speed permanent magnet motor,” Heliyon, vol. 8, 2022, Art. no. e11350, doi: 10.1016/j.heliyon.2022.e11350.

[16] K. Sim, Y.-B. Lee, S.-M. Jang, and T.H. Kim, “Thermal analysis of high-speed permanent magnet motor with cooling flows supported on gas foil bearings: Part I - coupled thermal and loss modelling,” Journal of Mechanical Science and Technology, vol. 29, no. 12, pp. 5469–5476, 2015, doi: 10.1007/s12206-015-1148-0.

[17] J. Dong, Y. Huang, L. Jin, H. Lin, and H. Yang, “Thermal optimization of a high-speed permanent magnet motor,” IEEE Transactions on Magnetics, vol. 50, no. 2, Feb. 2014, Art. no. 7018504, doi: 10.1109/TMAG.2013.2285017.

[18] Y. Choo, et al., “Investigation of systematic efficiency in a high-speed single-phase brushless DC motor using multi-physics analysis for a vacuum cleaner,” IEEE Transactions on Magnetics, vol. 55, no. 7, July 2019, Art. no. 8203606, doi: 10.1109/TMAG.2019.2903445.

[19] W. Hwang, J. Kim, J. Han, W. Kang, and S. Park, “Investigation of resonance avoidance method for vacuum cleaner,” IEEE Open Journal of Industry Applications, vol. 4, pp. 328–335, 2023, doi: 10.1109/OJIA.2023.3323343.

[20] M. Xu, Z. Qiu, and Z. Wang, “Research on weakening control strategy of permanent magnet synchronous motor of high speed vacuum cleaner based on sliding mode observer,” in Proc. Int. Conf. on Computers, Information Processing and Advanced Education, Ottawa, ON, Canada, 26-28 Aug. 2023, pp. 562–568, doi: 10.1109/CIPAE60493.2023.00112.

[21] S. Ok, Z. Xu and D. -H. Lee, “A sensorless speed control of high-speed BLDC motor using variable slope SMO,” IEEE Transactions on Industry

Applications, vol. 60, no. 2, pp. 3221-3228, Mar.-Apr. 2024, doi: 10.1109/TIA.2023.3348081.
[22] B. Jung, P. Jang, J. Kim, S. Lim and K. Nam, "Intermittent Inductance Estimation for High-Speed PMSM Sensorless Control," 2020 IEEE Applied Power Electronics Conf. Expo., 2020, pp. 248-252, doi: 10.1109/APEC39645.2020.9124188.
[23] W. Zhou, et al., "Inverter with paralleled modules to extend current capacity and combat motor overvoltage in SiC-based adjustable speed drives," IEEE Trans. Ind. Electron., vol. 71, no. 5, pp. 4474-4484, May 2024.
[24] W. Zhou, X. Yuan and Z. Zhang, "An active dv/dt filter to combat motor terminal overvoltage in SiC-based adjustable speed drives," IEEE Trans. Ind. Electron., vol. 72, no. 1, pp. 1076-1081, Jan. 2025.
[25] A. Dianov, "Inverter temperature monitoring of cordless tool motor drives." IEEE Open J. of the Ind. Electron. Soc., vol. 4, pp. 52-62, 2023.
[26] Dyson. "Dyson hyperdymium motor." [Online]. Available: https://www.dyson.co.uk/vacuum-cleaners/cordless/hyperdymium-motor.
[27] A. Dianov, "Stoppage noise reduction of reciprocating compressors," IEEE Trans. on Ind. Appl., vol. 57, no. 5, pp. 4376-4384, Sept./Oct. 2021.
[28] A. Dianov, "Instant closing of permanent magnet synchronous motor control systems at open-loop start," Sustainability, 14, 12665, pp. 1–18, Oct., 2022.
[29] M. -S. Lim, J. -M. Kim, Y. -S. Hwang and J. -P. Hong, "Design of an Ultra-High-Speed Permanent-Magnet Motor for an Electric Turbocharger Considering Speed Response Characteristics," IEEE/ASME Transactions on Mechatronics, vol. 22, no. 2, pp. 774-784, April 2017, doi: 10.1109/TMECH.2016.2634160.
[30] Z. Cui, Y. Le, K. Wang, H. Wang and S. Zheng, "A Low Rotor Eddy Current Loss Design Approach to HSPMSM for Small-Scale Magnetically Suspended Turbomolecular Pump," IEEE Trans. Ind. Electron., Early Access, doi: 10.1109/TIE.2024.3497316.
[31] T.R. He, F. Xu, Z.Q. Zhu, D. Liang, H. Bin, and D. Wu, "Comparison of toroidal and tooth-coil winding 2-pole slotted high-speed permanent magnet motors," IEEE Transactions on Industry Applications, vol. 60, no. 3, pp. 3870–3882, May-June 2024, doi: 10.1109/TIA.2024.3366500.
[32] N. Bianchi, S. Bolognani, and F. Luise, "Potentials and limits of high-speed PM motors," IEEE Transactions on Industry Applications, vol. 40, no. 6, pp. 1570-1578, Nov.-Dec. 2004, doi: 10.1109/TIA.2004.836173.
[33] N. Bianchi, S. Bolognani, and F. Luise, "Analysis and design of a PM brushless motor for high-speed operations," IEEE Transactions on Energy Conversion, vol. 20, no. 3, pp. 629-637, Sep. 2005, doi: 10.1109/TEC.2005.847991.
[34] F. Xu, et al., "Influence of slot number on electromagnetic performance of 2-pole high-speed permanent magnet motors with toroidal windings," IEEE Transactions on Industry Applications, vol. 57, no. 6, pp. 6023–6033, Nov.-Dec. 2021, doi: 10.1109/TIA.2021.311773.
[35] A. Dianov, "A novel phase loss detection method for low-cost motor drives." IEEE Trans. Power Electron., vol. 37, no. 6, pp. 6660-6668, Jun. 2022.

ANTON DIANOV (M'06–SM'18) received the BSc(hns.), MSc(hns.), and PhD degrees in electrical engineering from the National Research University "Moscow Power Engineering Institute", Moscow, Russia, in 2000, 2002, and 2005, respectively.

From 2005 to 2021, he was a Senior Engineer with Samsung Electronics, where he developed motor drives for home appliances. He is the author of more than 50 publications in the referring journals and conferences on electrical drives and motor control. He is the author of several patents on control algorithms for electrical drives and power electronics. He is a member of editorial board of several journals including IEEE OPEN JOURNAL OF THE INDUSTRIAL ELECTRONICS SOCIETY and IEEE JOURNAL OF EMERGING AND SELECTED TOPICS IN POWER ELECTRONICS. His research interests include electrical drives, sensorless, and advanced control algorithms.

Dr. Dianov was awarded with several personal scholarships including the scholarship form the President of Russian Federation and Wenzhou Ouyue outstanding high talent program award.

XIAODONG SUN (M'12-SM'18) received the B.Sc. degree in electrical engineering, and the M.Sc. and Ph.D. degrees in control engineering from Jiangsu University, Zhenjiang, China, in 2004, 2008, and 2011, respectively.

Since 2004, he has been with Jiangsu University, where he is currently a Professor in Vehicle Engineering with the Automotive Engineering Research Institute. From 2014 to 2015, he was a Visiting Professor with the School of Electrical, Mechanical, and Mechatronic Systems, University of Technology Sydney, Sydney, Australia. His current teaching and research interests include electrified vehicles, electrical machines, electrical drives, and energy management. He is the author or coauthor of more than 100 refereed technical papers and one book, and he is the holder of 42 patents in his areas of interest. Dr. Sun is an Associate Editor of the IEEE TRANSACTIONS ON INDUSTRIAL ELECTRONICS, Associate Editor of the IEEE TRANSACTIONS ON TRANSPORTATION ELECTRIFICATION, and Editor of the IEEE TRANSACTIONS ON ENERGY CONVERSION.

RUI YANG born in Xiayi County, Henan Province, in 1970. Obtained a BSc degree in Metal Pressure Processing from Anhui University of Technology in July 1993, and a Master's degree in Mechatronic Engineering from Lanzhou University of Technology in July 2007, and received a Ph.D. in Fluid Machinery and Engineering from Lanzhou University of Technology in 2009.

Professor of Wenzhou University, Director of Wenzhou University Pingyang Intelligent Manufacturing Research Institute, Oujiang A-Class Professor of Wenzhou University. Dedicated to aerodynamics and applied research for over 20 years. Member of Wind Energy Committee, Chinese Renewable Energy Society, Wind Energy Aerodynamics Committee, Chinese Society of Aerodynamics, Chinese Renewable Energy Society Comprehensive Committee, Chinese Hydropower Engineering Society and Senior Member of Gansu Hydropower Engineering Society. Expert Consultant for China Huaneng Group, China Energy Conservation Group, and China Three Gorges Renewables. Led or participated in over 30 national/key projects, including National 973/863 Programs. Awarded Second Prize of China Machinery Industry Science and Technology Award and Second Prize of Gansu Provincial Science and Technology Progress Award.

JIAWEI XIANG (Senior Member, IEEE) (SM'2023) received the B.Sc. degree in mechatronics from Hunan University, China, in 1997, the M.Sc. and PhD degrees in mechanical engineering from Guangxi University, China, in 2003, and from Xi'an Jiaotong University, China, in 2006, respectively. He is currently a professor at the College of Mechanical and Electrical Engineering, Wenzhou University, China. His research interests are the condition monitoring of mechanical systems, structural health monitoring, numerical simulation, signal processing, and vibration analysis. He is also a Fellow of IET, Executive director of the Chinese Society of Vibration Engineering (CSVE), and a member of ASME.

YURIY VAGAPOV received the Dip. Eng. and Ph.D. degrees from Nizhny Novgorod State Technical University, Nizhny Novgorod, Russia, in 1982 and 1995 respectively. He is a Reader in Electrical Engineering at Glyndwr University, Wrexham, Wales, U.K. His academic interests are in the area of electrical engineering specifically power electronics, electrical machines and drives, and electric vehicles. He is a Chartered Engineer and member of the IET.